

This is the accepted manuscript made available via CHORUS. The article has been published as:

Contrasting the magnetism in
 $\text{La}_{2-x}\text{Sr}_x\text{FeCoO}_6$ ($x=0,1,2$) double perovskites:
The role of electronic and cationic disorder

G. R. Haripriya, C. M. N. Kumar, R. Pradheesh, L. M. Martinez, C. L. Saiz, S. R. Singamaneni, T. Chatterji, V. Sankaranarayanan, K. Sethupathi, B. Kiefer, and H. S. Nair

Phys. Rev. B **99**, 184411 — Published 13 May 2019

DOI: [10.1103/PhysRevB.99.184411](https://doi.org/10.1103/PhysRevB.99.184411)

Contrasting the magnetism in $\text{La}_{2-x}\text{Sr}_x\text{FeCoO}_6$ ($x = 0, 1, 2$) double perovskites: the role of electronic and cationic disorder

G. R. Haripriya,¹ C. M. N. Kumar,^{2,*} R. Pradheesh,¹ L. M. Martinez,³ C. L. Saiz,³ S. R. Singamaneni,³ T. Chatterji,⁴ V. Sankaranarayanan,¹ K. Sethupathi,¹ B. Kiefer,⁵ and H. S. Nair^{3,†}

¹*Low Temperature Physics Laboratory, Department of Physics,
Indian Institute of Technology Madras, Chennai, India*

²*Institut für Festkörperphysik, TU Wien,
Wiedner Hauptstr. 8-10/138, 1040 Wien, Austria*

³*Department of Physics, 500 W. University Ave,
University of Texas at El Paso, El Paso, TX 79968, USA*

⁴*Institut Laue-Langevin, BP 156, 38042 Grenoble Cedex 9, France*

⁵*Department of Physics, New Mexico State University, Las Cruces, New Mexico 88011, USA*

(Dated: April 19, 2019)

Abstract

The magnetism of the double perovskite compounds $\text{La}_{2-x}\text{Sr}_x\text{FeCoO}_6$ ($x = 0, 1, 2$) are contrasted using magnetization, neutron diffraction and electron paramagnetic resonance with the support from density functional theory calculations. $\text{La}_2\text{FeCoO}_6$ is identified as a long-range ordered antiferromagnet displaying a near-room temperature transition at $T_N = 270$ K, accompanied by a low temperature structural phase transition at $T_S = 200$ K. The structural phase transformation at T_S occurs from $R\bar{3}c$ at 300 K to $Pnma$ at 200 K. The density functional theory calculations support an insulating non-compensated AFM structure. The long-range ordered magnetism of $\text{La}_2\text{FeCoO}_6$ transforms to short-range glassy magnetism as La is replaced with Sr in the other two compounds. The magnetism of $\text{La}_2\text{FeCoO}_6$ is differentiated from the non-equilibrium glassy features of $\text{Sr}_2\text{FeCoO}_6$ and SrLaFeCoO_6 using the *cooling-and-heating-in-unequal-fields* (CHUF) magnetization protocols. This contrasting magnetism in the $\text{La}_{2-x}\text{Sr}_x\text{FeCoO}_6$ series is evidenced in electron paramagnetic resonance studies. The electronic density-of-states estimated using the density functional theory calculations contrast the insulating feature of $\text{La}_2\text{FeCoO}_6$ from the metallic nature of $\text{Sr}_2\text{FeCoO}_6$. From the present suite of experimental and computational results on $\text{La}_{2-x}\text{Sr}_x\text{FeCoO}_6$, it emerges that the electronic degrees of freedom, along with antisite disorder, play an important role in controlling the magnetism observed in double perovskites.

I. INTRODUCTION

Double perovskites $\text{Sr}_2BB'\text{O}_6$, where B/B' are transition metal elements, attracted attention due to the observation of large magnetoresistance in the case of $B/B' = \text{Fe}/\text{Mo}^{1-3}$. The cation-ordered $\text{Sr}_2\text{FeMoO}_6$ was reported to show room temperature, low-field magnetoresistance (MR) with the striking feature of scaling of MR with the square of spin-polarization of carriers, $(M/M_s)^2$, where M_s is the saturation magnetization¹. This suggested the potential for spintronics and giant magnetoresistance applications in an ideally ferromagnetic double perovskite lattice, which motivated experimental studies connected to the low-field MR in $\text{Sr}_2\text{FeMoO}_6^{2,4}$. However, double perovskites prepared at high temperatures in laboratories suffer from antisite disorder on the B/B' site. This leads to the disruption of the $B^{2+} - \text{O} - B'^{4+}$ magnetic exchange paths and consequent weakening of ferromagnetism predicted by the Goodenough-Kanamori rules for an ordered cation arrangement of cations^{5,6}. Antisite disorder has a strong bearing on the magnetic and the transport behaviour of the double perovskites. Significant differences in MR at low temperature (4.2 K) was reported in the case of ordered (degree of Fe/Mo ordering = 91%), versus the disordered (degree of Fe/Mo ordering = 31%) $\text{Sr}_2\text{FeMoO}_6$. Though the Fe/Mo-based $\text{Sr}_2BB'\text{O}_6$ was studied in detail for its magnetoresistive properties, less attention was paid to the Fe/Co based $\text{Sr}_2BB'\text{O}_6$ compounds which offer the possibility of tuning the structural, valence and spin-state parameters connected to the magnetic behaviour. This is particularly possible due to the presence of Co, which can adopt low-spin (LS), high-spin (HS) or intermediate-spin (IS) states depending on the valence that is stabilized in a particular double perovskite structure. The orbital degrees of freedom and consequently the spin-orbit coupling effects attain importance in this case.

It is, hence, understood that the crystallographic antisite disorder has a significant impact on the magnetism of double perovskites. Another important structural detail that has a significant bearing is the distortions of the metal-oxygen octahedra that constitute the perovskite. The ideal perovskite AMX_3 structure adopts highly symmetric cubic space group $Pm\bar{3}m$ where the A cation is surrounded by 12 X anions and the M cation by 6 X anions. The three-dimensional view of the perovskite structure is that of a corner-sharing MX_6 octahedra. Distortions, tilting or cation displacements in the octahedra lead to a deviation from the ideal cubic structure and can lead to low symmetry space groups like $P2_1/n$ or $I4/m$. A convenient classification of how the tilts in the perovskite structure leads to different space groups symmetries is provided by Glazer⁷. Using this system, a tilt in the octahedra is described by specifying the rotations of the octahedra about

each of the three cartesian axes. The $Pm\bar{3}m$ space group belongs to the tilt system $a^0a^0a^0$ and the rhombohedral space group $R\bar{3}c$, $a^-a^-a^-$. The rotation pattern of the orthorhombic $Pnma$ space group is determined by two tilts which are $a^0a^0a^+$ and $a^-a^-a^0$. The octahedral tilts and rotations are extremely important to single and layered perovskite compounds in bringing about novel type of ferroelectricity⁸. The double perovskite compounds are generally found to adopt random, rock salt or layered structure types depending on the degree of B cation arrangement⁹. Space groups $Pm\bar{3}m$ and $Pnma$ (random), $Fm\bar{3}m$, $P2_1/n$ (rock salt) and $P2_1/m$ (layered) were predicted based on this⁹.

The role of cation disorder in the crystal structure and magnetism of the $Sr_2BB'O_6$ compound Sr_2FeCoO_6 (SFCO) was investigated by some of us¹⁰. SFCO was seen to adopt the tetragonal space group $I4/m$ with the lattice parameters, $a = 5.4609(2)$ Å and $c = 7.7113(7)$ Å; which is about 2% reduced in the a and b compared to those of Sr_2FeMoO_6 . The magnetic ground state is identified as a canonical spin glass with a spin freezing temperature, $T_g \approx 75$ K,¹⁰ which is quite different from the ferrimagnetic ground state of Sr_2FeMoO_6 with a T_c in the range 410 – 450 K¹¹. Albeit the differences in the magnetic ground state and the lattice parameters, SFCO displays large magnetoresistance of 63% at 14 K in 12 T¹². Strong antisite disorder was observed in SFCO along with the presence of mixed valence states for Co. The disorder effect and mixed valence in SFCO gave rise to not only the spin glass magnetism, but also to large magnetoresistance derived from the spin scattering of the carriers localized by the magnetic moments in the spin glass state. Additionally, it also lead to the development of exchange bias¹³. Upon replacement of Sr with La in the case of $SrLaFeCoO_6$ (SLFCO), features of a magnetic glass were observed¹⁴. The magnetization of SLFCO showed an anomaly at $T_{a1} \approx 75$ K. Despite the non-equilibrium metastable magnetic state, significant magnetoresistance of about 47% was observed in SLFCO at 5 K in 8 T¹². With the addition of La, a significant change in the crystal structure was the stabilization of monoclinic space group $P2_1/n$. Although the monoclinic structure is amenable to perfect ordering of Fe and Co in two different Wyckoff positions $2c$ and $2d$, a high degree of disorder ($\approx 90\%$) was observed in SLFCO.

The present paper extends the work on SFCO and SLFCO to the crystal structure and magnetism of La_2FeCoO_6 (LFCO). Using the experimental tools of magnetization, neutron diffraction and electron paramagnetic resonance (EPR) we study the structure and magnetism in LFCO and compare it with that of SFCO and SLFCO. Density functional theory (DFT) calculations on all the three compounds support our experimental findings. It is seen that LFCO develops magnetic

long-range order at significantly high temperatures (≈ 270 K) and subsequently undergoes a structural phase transition at 200 K. The magnetism in LFCO is opposed to that of SFCO and SLFCO, which are seen to be magnetically disordered below ≈ 75 K.

II. METHODS

A. Experimental techniques

Polycrystalline samples of $\text{La}_2\text{FeCoO}_6$ were prepared following sol-gel method as described in Reference [10], which explains the preparation of SFCO. For the present work, LFCO and SLFCO were prepared using a similar synthesis method. The synthesized compounds were first analyzed using powder X-ray diffraction to check phase purity and crystal structure. Magnetic measurements were carried out on pressed pellets in a Magnetic Property Measurement system SQUID Vibrating Sample Magnetometer (MPMS-SVSM) in the temperature range, 5 – 350 K and magnetic field ± 7 T. Zero field cooling (ZFC), field-cooled warming (FCW) and field cooled cooling (FCC) protocols were used to measure dc magnetization. Neutron powder diffraction experiments on LFCO and SLFCO were performed at WISH (Rutherford Appleton Laboratory, UK)¹⁵. Roughly 8 g of well-characterized powder sample was used for each neutron experiment. The diffraction data was analyzed using Fullprof Suite of programs¹⁶ for Rietveld refinements and the software SARA h ¹⁷ was used for the analysis of magnetic structure using representation analysis. EPR data were recorded on a Bruker EMX Plus X-band (≈ 9.43 GHz) spectrometer, equipped with a high sensitivity probe head. A ColdEdgeTM ER 4112HV In-Cavity Cryo-Free VT system connected with an Oxford temperature controller was used for low temperature measurements.

B. Computational methods

We first present the results of the parameter-free first-principles density functional theory computations^{18,19} to elucidate the structure and magnetism in the series of three compounds $\text{Sr}_2\text{FeCoO}_6$, SrLaFeCoO_6 and $\text{La}_2\text{FeCoO}_6$. Our calculations take into account the experimental low temperature crystal structure details and hence are more reliable than the previous reports. All computations were performed for the relevant low temperature structures, obtained from our neutron experiments. All computations were performed for fixed lattice and positions. We determined electronic and magnetic properties for SFCO, SLFCO and LFCO, for fixed structure, neglecting

relaxation effects of any crystallographically allowed degrees of freedom. All computations were performed with the 3D planewave software package VASP²⁰⁻²² with the projector-augmented wave method^{23,24} with the PBE-GGA exchange correlation functional²⁵ and included on-site Coulomb interactions (DFT + U)²⁶. $U = 5.0$ eV for Fe and Co, $E_{\text{cut}} = 400$ eV and a k -point spacing of 0.25 were used for all computations, similar to the previous work on LFCO²⁷ and related compounds²⁸⁻³⁰. The k -point density ensured that it was sampled homogeneously across different crystal structures, facilitating a comparison of computed properties. For Sr, La, Fe, Co, and O, we considered explicitly $5s^24p^64s^2$, $5d^16s^25p^65s^2$, $3d^64s^1$, $3d^74s^2$, and $2s^22p^4$ as shells in our computations, respectively. In order to explore the effect of spin-lattice coupling and the robustness of the electronic structure in the vicinity of the Fermi energy, we included spin-orbit coupling in the most stable configurations and in order to resolve better the small effects of spin-orbit coupling we used a denser Γ -centered k -point grid with a spacing of 0.15.

III. RESULTS

A. Density functional theory of $\text{La}_{2-x}\text{Sr}_x\text{FeCoO}_6$

1. $\text{La}_2\text{FeCoO}_6$

The electronic density of states (eDOS) for all the three compositions of $\text{La}_{2-x}\text{Sr}_x\text{FeCoO}_6$ are presented in Fig 1. We tested the oxidation states of all three compounds with different cation distributions denoted as A, C, and G, adopting the labeling of magnetic structures in perovskites³¹. If the two Fe ions are in the same plane perpendicular to the long axis, we refer to an A-structured arrangement (4 Fe and 2 Co nearest neighbors); if the two Fe ions are on a line parallel to the long axis, they form a C-structured arrangement (2 Fe and 4 Co nearest neighbors); if all nearest-neighbors are of opposite type, they are labeled as G-structured arrangement (0 equal and 6 non-equal neighbors). In the case of $\text{La}_2\text{FeCoO}_6$, total energy differences between A, C, and G transition metal arrangements are less than 9.0 meV/5 atoms, consistent with strong (Fe,Co) antisite disorder. This is approximately an order of magnitude smaller in energy than computed for $\text{Ba}_x\text{Sr}_{1-x}\text{Co}_y\text{Fe}_{1-y}\text{O}_{3-\delta}$, where a single (Fe,Co) exchange requires 80 meV³². The ground state is G-structure and insulating. The computed magnetic structure corresponds to non-compensated AFM with site projected magnetic moments of +4.2, +4.2, -3.1, -3.1 μ_B , for Fe and Co (Fig. 1 (a)). The magnetic moments are consistent with Fe^{2+} (HS) and Co^{4+} (IS) charge assignments, as

reported before²⁷, except that our magnetic ground state is not FM, but non-compensated AFM as described recently³³. All structure/oxidation states/magnetic moment arrangements converged to the same oxidation state, described above. Thus, no valence disorder is required to explain the magnetic ground state of LFCO. Similarly, A-, and C- structured transition metal arrays form excited states. They are AFM with magnetic moments of +4.2, -4.2, -3.1, +3.1 μ_B , and 9 meV/5 atoms and 3 meV/5 atoms higher than the predicted to be non-compensated AFM. This near-degeneracy of states may explain the small hysteresis in the magnetization curve of LFCO (Fig. 2 (b)). A-, C-, G-plaquettes are randomly generated at the high synthesis temperature ($T > 1000^\circ$ C) and form the structural template for LFCO. If so, the magnetic state is likely a superposition of non-compensated AFM and AFM structure at low temperature. Moreover, CHUF2 observations (presented in Section III D) suggest unsaturated magnetic moments, in general agreement with our computed results. The small energy differences do suggest that spin-orbit coupling may influence the magnetic structure. Our results show that energy differences between different spin orientations are 1 meV/5 atoms. We find that spins sub-parallel to the [001] direction are energetically most favorable, followed by [010] and [111] magnetization directions. The orbital and spin moments for the most stable [001] magnetic structure are parallel for Fe, as expected from Hund's rules for less than half-filled electron shells ($3d^4$). Interestingly, we find an orbital moment for Co, suggesting that Co^{4+} is not in a high-spin state ($3d^5$). However, the orbital moments are at least two orders of magnitude smaller than the spin magnetic moments, but support a small canting confined to the bc -plane, consistent with our neutron scattering data (Section III C).

2. SrLaFeCoO_6

In the case of SLFCO, the DFT ground state is AFM with a G-type transition and a C-type Sr, La arrangement and site-projected magnetic moments of +3.9, -3.9, -2.8, +2.8 μ_B , and semi-metallic electronic structure (Fig. 1 (b)). In an ionic picture $q(\text{Fe}) + q(\text{Co}) = 7$. The magnetic moments are consistent with Fe^{2+} (HS) and Fe^{4+} (HS), leaving Co in a +5 or +3 charge state, with even magnetic moments, in contrast to the computed moment. This discrepancy may be attributed to charge ordering, and the coexistence of Co^{5+} (HS) and Co^{3+} (IS) states suggesting the presence of mixed valence states¹⁰. Moreover, we find that the second most stable phase is FM with the same cation arrangement as the ground state, but ~ 1.5 meV/5 atoms less stable. The site projected magnetic moments are +4.0, +4.0, +2.0, +3.0 μ_B , for Fe, and Co, respectively. The

magnetic moments of one of the Co atoms is predicted to decrease by $\sim 1 \mu_B$, as compared to the ground state, and consistent with a charge assignment of $\text{Co}^{3+}(\text{IS})$, and $\text{Co}^{5+}(\text{IS})$. The existence of a low lying FM state is in excellent agreement with the interpretation of our magnetometry (Section III D) and our EPR results (Section III E).

3. $\text{Sr}_2\text{FeCoO}_6$

For SFCO, the DFT computations show that the ground state is an antiferromagnetic metal (Fig 1 (c)), with G-type transition metal ion and spin arrangement. The cell magnetic moment (20 atoms) is zero and the site projected magnetic moments are $+3.7 \mu_B$, $-3.7 \mu_B$, $-2.9 \mu_B$, $+2.9 \mu_B$ for Fe and Co respectively, in overall agreement with our experimental observations. The second most stable state predicted is ferromagnetic with C-type arrangement, and 4 meV/5 atoms less stable than the antiferromagnetic ground state, and a magnetic moment is $10.6 \mu_B/20$ atoms. Given the small energy difference it is to be expected that G-type and C-type structural plaquettes can coexist at the high synthesis temperatures. More importantly, we note that the magnitude of the site-projected magnetic moments are $3.8 \mu_B$, $4.0 \mu_B$, $2.8 \mu_B$, and $2.9 \mu_B$, for the two Fe and Co atoms, respectively. Regardless of the initialized multiplet in the computations, the magnitude of the final spins was always within $0.3 \mu_B$ of the ground state, supporting a common oxidation state. A consistent set of oxidation states is $\text{Fe}^{4+}(\text{HS})$ and $\text{Co}^{4+}(\text{IS})$, and similar to LFCO, the DFT results do not require valence state mixing for SFCO. Therefore, the DFT computations suggest that magnetic multiplets are energetically close and can coexist at low temperatures, leading to a broadened EPR signal, and enabling a complex magnetic state. With this backdrop of the structure, electronic density-of-states and the magnetic structures determined, we now take a look at the magnetism of the three $\text{La}_{2-x}\text{Sr}_x\text{FeCoO}_6$ compounds reflected in experiments.

B. $\text{La}_2\text{FeCoO}_6$: Magnetization

Macroscopic magnetization of $\text{La}_2\text{FeCoO}_6$ measured using ac and dc magnetometry are presented in Fig 2. The ac susceptibility, $\chi(T)$, in the frequency range 1 Hz to 999 Hz and temperature range 200 K–300 K is shown in the panel (a). A magnetic phase transition at $T_N \approx 270$ K is clearly seen in Fig 2 (a). A weak frequency dependence of susceptibility is observed at T_N . In Fig 2 (a), a

significant reduction in the magnetization is observed at $T \approx 200$ K. The features in magnetization correlates with the structural phase transition in LFCO from $R\bar{3}c$ to $Pnma$ which is described in detail in the next subsection. The isothermal magnetization curves at 5 K, 20 K, 150 K, 225 K and 300 K are shown in Fig 2 (b). The magnetization isotherms in (b) show hysteresis at low temperatures, especially at 20 K and 5 K. However, the maximum magnetic moment attained at 5 K with the application of 7 T is $\mu_{\max} \approx 0.2 \mu_B/\text{f.u.}$ We note that our DFT computations described above are consistent with the macroscopic magnetization measurements if the magnetic domains are randomly oriented. The dc magnetization measurements shown in (c) support the magnetic transition at T_N . A large irreversibility between the ZFC and FCW curves of magnetization is observed. Additionally, a strong thermal hysteresis of the FCC and FCW curves is seen around 200 K. It is revealed later in the next section that it is a structural transition that causes the thermal hysteresis and the large irreversibility. The magnetic phase transition in the present case occurs close to 300 K while our measurement capability was limited upto 350 K thereby not permitting a Curie-Weiss analysis in a large paramagnetic range.

C. $\text{La}_2\text{FeCoO}_6$: Neutron diffraction

In order to understand the magnetic structure of $\text{La}_2\text{FeCoO}_6$ that would explain the magnetization features observed in Fig 2, we performed neutron diffraction experiments. The results are presented in Fig 3. A magnetic anomaly at $T_N \approx 270$ K can be discerned from (a) where the development of an additional Bragg peak at $d \approx 4.5 \text{ \AA}$ occurs. This feature relates to the (011) and (110) Bragg peaks which is indicative of an AFM magnetic structure of the G type. The Rietveld refinement of the diffraction pattern at 300 K is shown in panel (b) where the experimental intensity is plotted in red circles and the calculated as black solid line. The crystal structure of LFCO at 300 K is refined in the rhombohedral space group, $R\bar{3}c$ with the lattice parameters $a = 5.4935(2) \text{ (\AA)}$ and $c = 13.2343(2) \text{ (\AA)}$. A structural phase transition is observed in LFCO at $T_S \approx 200$ K where the crystal structure transforms from $R\bar{3}c$ to orthorhombic $Pnma$. Presented in Fig 3 (c) is a plot of the percentage phase fraction of the two structural phases as a function of temperature. In the intermediate temperature region centered around 200 K, mixed structural phases exist. In the inset of Fig 3 (b), the bond angle $\langle \text{Co-O-Fe} \rangle$ and in the inset of (c), the bond distance $d_{\text{Fe/Co-O}}$ in $\text{La}_2\text{FeCoO}_6$ are shown. Both the bond angles and the bond distances reflect strong anomalies around T_S where the structural phase transition occurs. The thermal hysteresis

in magnetization and the large bifurcation in the ZFC/FC curves in LFCO is due to the coexistence of mixed $R\bar{3}c$ and $Pnma$ phases over a large temperature range, having different magnetization responses to an external magnetic field.

As the temperature is reduced to 1.5 K, the magnetic Bragg peaks (011) and (110) are enhanced in the diffraction pattern, see Fig 3 (d). This corresponds to the Bragg intensity that develops at $d = 4.5 \text{ \AA}$ at the T_N , Fig 3 (a). The nuclear structure of LFCO at 1.5 K retains the $Pnma$ symmetry. The magnetic structure of LFCO was solved after determining the propagation vector through a profile fit to the low temperature magnetic peaks ((011) and (110)), thus obtaining $k (0\ 0\ 0)$. The k-search utility within the FullProf Suite was used for this purpose. Using this propagation vector, the symmetry-allowed magnetic representations for LFCO were determined using SARA h ¹⁷. The crystal structure was assumed to be a pure phase of $Pnma$ in this case and the magnetic moments of Fe and Co were assumed to be same since they occupy the same crystallographic position within the unit cell. The best description to the observed diffraction data was obtained with the Γ_5 representation ($Pn'ma'$, BNS label 62.448). A schematic of the arrangement of the magnetic moments in the unit cell in Γ_5 representation is shown in the inset of Fig 3 (d), which shows the $F_y G_z$ AFM structure. During the course of refinement, magnetic moment components were allowed to vary along all crystallographic directions, however, a negligible value was obtained for the x -component of the magnetic moment. Absence of a spin re-orientation transition at high temperatures was confirmed and subsequently, the magnetic moments were restricted to be in the y and z directions only in agreement with the DFT calculations. After refining the magnetic moments at 4 K, we obtained ordered moment of $1.89(7)\mu_B/(\text{Fe,Co})$ atoms. The structural parameters extracted from the Rietveld refinement of neutron diffraction patterns at 300 K and 1.5 K are presented in Table I.

D. CHUF magnetization of $\text{La}_{2-x}\text{Sr}_x\text{FeCoO}_6$

From the above sections it is clear that the magnetism of $\text{La}_2\text{FeCoO}_6$ is different from the disordered magnetism found in $\text{Sr}_2\text{FeCoO}_6$ and SrLaFeCoO_6 ^{10,14}. In order to contrast the magnetism in the three compounds, we performed detailed protocol-based magnetization measurements. Cooling-and-heating-in-unequal-fields (CHUF) protocol is a useful magnetization protocol which can be used to record magnetization curves as a function of temperature in order to differentiate the non-equilibrium nature of the *glass-like* magnetic features from that of an equilibrium

response³⁴⁻³⁶. In what we term as CHUF1 protocol, the sample is cooled across the transition temperature in a certain applied magnetic field H_C . At the lowest temperature, H_C is isothermally changed to a different value of measuring field and the magnetization is measured while warming the sample. The result of this measurement protocol for LFCO, SLFCO and SFCO are presented in (a), (b) and (c) respectively in Fig 4. The magnetic field used to measure the magnetization in the warming cycle is notated as H_W in the figure. Several values of external magnetic fields 0 T, 0.05 T, 0.1 T, 1 T, 3 T and 5 T were used as H_C to cool the samples (see, (a), (b), (c)). In all the three cases, $H_W = 2$ T was used to measure the magnetization while warming. In a second protocol, CHUF2, the cooling field H_C was kept constant at 2 T during the time the sample was cooled down to low temperature and, subsequently, different fields of H_W were used in the warming cycle to measure the magnetization. The results of this protocol are presented in (d), (e) and (f) of Fig 4 for LFCO, SLFCO and SFCO, respectively. In the case of LFCO which orders long-range at high temperature, no signature of magnetic relaxation or non-equilibrium dynamics is seen in the CHUF1 measurement in (a). Note that a H_C upto 5 T and a warming field of 2 T does not affect the magnetization features. However, apart from a discontinuity in the magnetization at $T_N \approx 270$ K, a second anomaly is discernible at $T_S \approx 200$ K in LFCO, coinciding with the structural transformation between $R\bar{3}c$ and $Pnma$ phases. The CHUF measurement reveals that LFCO behaves in the same way for the $H_C > H_W$ and $H_C < H_W$ regimes and hence a magnetic glass-like state can be ruled out. In the case of CHUF2 protocol, we see that the magnetization increases with higher value of measuring fields for H_W . The anomalies at 270 K and 200 K are still present however, with the application of 3 T and 5 T for H_W , the magnetization at low temperature is enhanced. In the case of SLFCO, the CHUF1 protocol shows contrasting effects for the two cases, $H_C > H_W$ and $H_C < H_W$, as seen in (b). When the cooling field is larger than the measuring field, *i.e.*, when $H_C > H_W$, the magnetization below the anomalous temperature $T_{a1} \approx 75$ K is significantly increased. This observation is consistent with a kinetically arrested ferromagnetic state of SLFCO. When SLFCO is warmed up, this glass-like arrested ferromagnetic phase reverts to the equilibrium antiferromagnetic phase. In the CHUF2 protocol for SLFCO shown in the figure panel (e), we can see that the magnetization tends to increase in magnitude with higher values of H_W . Note that there is a drastic difference in the magnetization profile below T_{a1} when the CHUF1 and CHUF2 curves of SLFCO are compared. From Fig 4 (e) it is clear that when $H_W > H_C$, the weak anomaly seen below T_{a1} vanishes and a higher magnetization is resulted. The features seen in (b) and (e) confirm that SLFCO has a glass-like mixed phase where a large

volume fraction of the ferromagnetic phase devitrifies. In the case of SFCO, the CHUF1 and the CHUF2 data presented in the figures (c) and (f) respectively show signs of magnetic relaxation similar to that of SLFCO albeit weaker in magnitude. The CHUF1 protocol in (c) do indicate that the magnetization for $H_C > H_W$ shows an enhanced magnitude below the T_g .

E. Electron paramagnetic resonance of $\text{La}_{2-x}\text{Sr}_x\text{FeCoO}_6$

As another experimental tool to contrast the magnetism in the three compounds, we use electron paramagnetic resonance (EPR). The differing features of the magnetic ground states of SFCO, SLFCO and LFCO are consistent with the EPR observations presented in Fig 5 (a-c), where the EPR signals at 20 K, 40 K, 60 K, and at 300 K are plotted. The EPR spectra showed a dramatic dependence on La and Sr composition in the present series of compounds, consistent with magnetization and neutron diffraction results. Figure 5 (a) plots the temperature evolution of EPR spectrum measured at 20 K, 40 K, 60 K and 300 K for LFCO. For LFCO at 300 K, we observe two distinct EPR signals. The first signal at $g = 2.05(6)$ (the central field, $H_0 = 3266$ G) associated with the peak-to-peak line width (ΔH_{pp}) of 3266 G, and the second signal appears at $g = 0.76(9)$ ($H_0 = 8728$ G). We believe that the former signal is due to the strongly exchange coupled Fe^{3+} and Co^{2+} spins, whereas the latter one was found to originate from the cavity background, and hence is discarded from further discussion. Because of the presence of the two signals, a broad Lorentzian curve does not completely account for the EPR linshape of LFCO at 300 K as can be understood from Fig 5 (a). It can be immediately noticed that as we lower the sample temperature from 300 K, a dramatic shift in the EPR signal toward the low field region occurs. At 60 K, we detected a complete signal associated with g value of 16.07 ($H_0 = 418$ G), characterized by ΔH_{pp} of 552 G. These are the benchmark signatures of an ordered antiferromagnetic phase. As we started to replace Sr in place of La in LFCO, the EPR signal broadens and shifts to the high field region, which becomes particularly noticeable at low temperatures (b and c panels). Furthermore, the disordered magnetic phase increases in abundance upon increasing the Sr content. For all the samples, as the temperature increases, the EPR signal gets sharper due to motional narrowing effect. Both (b) SLFCO and (c) SFCO appear to contain at least two magnetic phases that can give rise to spin glass-like behavior, which is consistent with our magnetometry results^{10,14}. The DFT computations also suggested that magnetic multiplets are energetically close in these compounds and can coexist at low temperatures and also at elevated magnetic fields, thereby leading to a broad-

ened EPR signal, enabling a complex magnetic state. It can be noted that the EPR response of the $\text{La}_{2-x}\text{Sr}_x\text{FeCoO}_6$ compounds are qualitatively different from that of $\text{Sr}_2\text{FeMoO}_6$ in which strong evidence of localized Fe^{3+} cores and itinerant Mo^{5+} electrons are found^{37,38} consistent with our DFT results that suggest Fe^{4+} . The g values and the H_{pp} values estimated from the EPR curves are shown in Table II. We have attempted to fit (not shown) the experimental EPR signal to a broad Lorentzian function of the form, $\frac{dP}{dH} = A \frac{d}{dH} [\Delta H / (4(HH_0)^2 + \Delta H^2) + \Delta H / (4(H + H_0)^2 + \Delta H^2)]$, where ΔH is the full-width-at-half-maximum which when divided by $\sqrt{3}$ gives the peak-to-peak linewidth ΔH_{pp} , and A is proportional to the area under the curve. Since the fits were not of high quality due to the presence of more than one lineshape terms in the data and also because the lineshapes were seen shifted more towards the negative field values as in the case of LFCO, they are not presented here.

IV. DISCUSSION AND CONCLUSIONS

In this section we want to discuss the present results in the light of the recent insight we obtained from high-resolution inelastic neutron scattering experiments to study the hyperfine interactions in SFCO, SLFCO and LFCO³⁹. It was shown that the inelastic signals observed in the two structurally and magnetically disordered compounds, SFCO and SLFCO were very broad, suggesting a distribution of hyperfine fields in these two materials whereas, no inelastic signal was observed in the case of LFCO. This suggested no or very weak hyperfine field at the Co nucleus due to the Co electronic moment. The inelastic spectra of SFCO were observed to be significantly narrow which could be attributed to a weaker hyperfine local field at the Co nucleus. An assumption of heterogeneous local fields at the Co nucleus due to the antisite disorder is consistent with SFCO which is a spin glass. The results from inelastic studies are in conformity with this picture and the model fits to the inelastic spectra suggests a finite energy splitting of $\approx 1 \mu\text{eV}$ (for details of the fits, please see Ref [39]).

The case of SLFCO appeared interesting as indications of electronic spin fluctuations in nano-second time scales were observed in the low- Q region, visible in the quasi-elastic channel, confirming magnetic short-range order and electronic spin freezing below 80 K. From the perspective of inelastic neutron scattering, the most surprising result was the absence of inelastic signal in the ordered state of $\text{La}_2\text{FeCoO}_6$ down to 1.8 K. This implies that the hyperfine field at the Co nucleus for this material is extremely weak to measure and that the Co moments may not be frozen at very

low temperatures. Thus we surmise that the observed magnetic properties of SFCO, SLFCO and LFCO are not easily explained solely based on the presence of antisite disorder. It is clear that the valence state disorder also plays an important role as we observe quasi-elastic scattering near the spin freezing temperatures which suggest fluctuations in the nanosecond time scale. With the addition of Sr in $\text{La}_2\text{FeCoO}_6$, the spin fluctuations slow down and lead to glassy dynamics which is observed through magnetometry. While it is beyond our computations to address antisite disorder directly, our results do suggest that C- and G-structured transition metal arrangements are likely to coexist.

An interesting progression of magnetic ground states is observed in $\text{La}_{2-x}\text{Sr}_x\text{FeCoO}_6$ as a function of the degree of disorder and with the replacement of La with Sr. $\text{La}_2\text{FeCoO}_6$ has a high temperature magnetic transition at $T_N \approx 270$ K and also a structural phase transition at $T_S \approx 200$ K where the compound transforms from $R\bar{3}c$ to $Pnma$. LFCO forms the only magnetically long-range ordered member in the series, whereas SFCO and SLFCO are magnetically disordered and form respectively, a spin glass and a magnetic glass with a spin freezing temperature, $T_g \approx 75$ K. The structural sensitivity at ≈ 200 K in LFCO is reflected in the other two compounds SLFCO and SFCO as a weak anomaly in the temperature dependence of lattice parameters and the magnetization. Our neutron diffraction results provide ample evidence of magnetic diffuse scattering persisting in SLFCO upto 300 K. From the CHUF magnetization protocols, electron paramagnetic resonance and neutron diffraction experiments, we mark SLFCO as a magnetic glass where nano scale spin fluctuations are evidenced through our recent inelastic neutron scattering work. Density functional theory calculations performed by adopting the crystal structure from the neutron diffraction predicts a AFiM/AFM ground state which is consistent with the antiferromagnetic state arrived at for LFCO through neutron scattering analysis. The magnitude of the magnetic moments remained the same as in LFCO, however, charge neutrality suggests the presence of mixed valence states, in contrast to LFCO and SFCO. These results align well with the overall picture obtained from our experiments for the three compounds from recent inelastic scattering experiments where the hyperfine fields of Co was modeled in detail. Our present work points toward the importance of competing valence state and spin state disorder in realizing different magnetic ground states in $\text{La}_{2-x}\text{Sr}_x\text{FeCoO}_6$ double perovskites. Even though our simulation cell (20 atoms) is not large enough to address the spin-glass state directly, it provides several insights, that distinguish LFCO from SLFCO. Both compositions show strong antisite disorder that can support different magnetic signatures. While the DFT findings do not provide conclusive evidence for a spin-glass state in

SFCO and SLFCO, they do suggest that the mechanism for spin-glass formation in SLFCO may be facilitated by valence state mixing, while in SFCO, it may be attributed to coexisting transition metal arrangements and antisite disorder.

V. ACKNOWLEDGEMENTS

HSN acknowledges the UTEP start-up funds and Rising-STARS award in supporting this work. BK would like to acknowledge computing resources provided through the National Science Foundation (XSEDE) under grant No. DMR TG-110093. CMNK acknowledges the financial support by FWF project P27980-N36 and the European Research Council (ERC Consolidator Grant No 725521). SRS, CLS and LMM acknowledge UTEP Start-up funds in supporting this work, and National Science Foundation (NSF), USA, with NSF-PREM grant DMR-1205302. LMM acknowledges the Wiemer Family for awarding Student Endowment for Excellence. The authors thank S. R. J. Hennadige for his help in doing EPR measurements. HGR, PR, KS and VSN acknowledge IITM for funding SVSM.

* naveen.chogondahalli@ifp.tuwien.ac.at

† hnair@utep.edu

- ¹ K. I. Kobayashi, T. Kimura, H. Sawada, K. Terakura, and Y. Tokura, *Nature* **395**, 677 (1998).
- ² D. D. Sarma, E. V. Sampathkumaran, S. Ray, R. Nagarajan, S. Majumdar, A. Kumar, G. Nalini, and T. N. Guru Row, *Solid State Commun.* **114**, 465 (2000).
- ³ D. D. Sarma, *Curr. Opinion Solid State and Mater. Sci.* **5**, 261 (2001).
- ⁴ J. Navarro, L. Balcells, F. Sandiumenge, M. Bibes, A. Roig, B. Martinez, and J. Fontcuberta, *J. Phys.: Condens. Matter* **13**, 8481 (2001).
- ⁵ J. Kanamori, *J. Phys. Chem. Solids* **10**, 87 (1959).
- ⁶ J. B. Goodenough, *Phys. Rev.* **100**, 564 (1955).
- ⁷ A. M. Glazer, *Acta Crystallogr. B* **28**, 3384 (1972).
- ⁸ N. A. Benedek, A. T. Mulder, and C. J. Fennie, *J. Solid State Chem.* **195**, 11 (2012).
- ⁹ M. T. Anderson, K. B. Greenwood, G. A. Taylor, and K. R. Poeppelmeier, *Prog. Solid State Chem.* **22**, 197 (1993).

- ¹⁰ R. Pradheesh, H. S. Nair, C. M. N. Kumar, J. Lamsal, R. Nirmala, P. N. Santhosh, W. B. Yelon, S. K. Malik, V. Sankaranarayanan, and K. Sethupathi, *J. Appl. Phys.* **111**, 053905 (2012).
- ¹¹ F. K. Patterson, C. W. Moeller, and R. Ward, *Inorg. Chem.* **2**, 196 (1963).
- ¹² R. Pradheesh, H. S. Nair, V. Sankaranarayanan, and K. Sethupathi, *Euro. Phys. J. B* **85**, 1 (2012).
- ¹³ R. Pradheesh, H. S. Nair, V. Sankaranarayanan, and K. Sethupathi, *Appl. Phys. Lett.* **101**, 142401 (2012).
- ¹⁴ R. Pradheesh, H. S. Nair, G. R. Haripriya, A. Senyshyn, T. Chatterji, V. Sankaranarayanan, and K. Sethupathi, *J. Phys.: Condens. Matter* **29**, 095801 (2017).
- ¹⁵ L. C. Chapon, P. Manuel, P. G. Radaelli, C. Benson, L. Perrott, S. Ansell, N. J. Rhodes, D. Raspino, D. Duxbury, E. Spill, et al., *Neutron News* **22**, 22 (2011).
- ¹⁶ J. Rodriguez-Carvajal, *Fullprof Suite*, <http://www.ill.eu/sites/fullprof/> (2017).
- ¹⁷ A. S. Wills, *Physica B* **276**, 680 (2000).
- ¹⁸ P. Hohenberg and W. Kohn, *Phys. Rev.* **136**, B864 (1964).
- ¹⁹ W. Kohn and L. J. Sham, *Phys. Rev.* **140**, A1133 (1965).
- ²⁰ G. Kresse and J. Hafner, *Phys. Rev. B* **48**, 13115 (1993).
- ²¹ G. Kresse and J. Furthmüller, *Comput. Mater. Sci.* **6**, 15 (1996).
- ²² G. Kresse and J. Furthmüller, *Phys. Rev. B* **54**, 11169 (1996).
- ²³ P. E. Blöchl, *Phys. Rev. B* **50**, 17953 (1994).
- ²⁴ G. Kresse and D. Joubert, *Phys. Rev. B* **59**, 1758 (1999).
- ²⁵ J. P. Perdew, K. Burke, and M. Ernzerhof, *Phys. Rev. Lett.* **77**, 3865 (1996).
- ²⁶ S. L. Dudarev, G. A. Botton, S. Y. Savrasov, C. J. Humphreys, and A. P. Sutton, *Phys. Rev. B* **57**, 1505 (1998).
- ²⁷ H.-R. Fuh, K.-C. Weng, C.-R. Chang, and Y.-K. Wang, *J. Appl. Phys.* **117**, 17B902 (2015).
- ²⁸ H. Wu, Y. Qian, W. Tan, C. Xiao, K. Deng, and R. Lu, *Appl. Phys. Lett.* **99**, 123116 (2011).
- ²⁹ J. M. Pruneda, J. Íñiguez, E. Canadell, H. Kageyama, and M. Takano, *Phys. Rev. B* **78**, 115101 (2008).
- ³⁰ Z. Yang, Z. Huang, L. Ye, and X. Xie, *Phys. Rev. B* **60**, 15674 (1999).
- ³¹ E. O. Wollan and W. C. Koehler, *Phys. Rev.* **100**, 545 (1955).
- ³² M. M. Kuklja, Y. A. Mastrikov, B. Jansang, and E. A. Kotomin, *J. Phys. Chem. C* **116**, 18605 (2012).
- ³³ W. Wang, W. Feng, J. Yuan, N. Pang, X. Zhao, M. Li, Z. Bao, K. Zhu, and D. Odkhuu, *Physica B* **540**, 33 (2018).
- ³⁴ P. Kushwaha, A. Lakhani, R. Rawat, and P. Chaddah, *Phys. Rev. B* **80**, 174413 (2009).
- ³⁵ A. Banerjee, K. Kumar, and P. Chaddah, *J. Phys.: Condens. Matter* **21**, 026002 (2009).

- ³⁶ S. B. Roy and M. K. Chattopadhyay, Phys. Rev. B **79**, 052407 (2009).
- ³⁷ D. Niebieskikwiat, R. D. Sánchez, A. Caneiro, L. Morales, M. Vásquez-Mansilla, F. Rivadulla, and L. E. Hueso, Phys. Rev. B **62**, 3340 (2000).
- ³⁸ M. Tovar, M. Causa, A. Butera, J. Navarro, B. Martínez, J. Fontcuberta, and M. Passeggi, Phys. Rev. B **66**, 024409 (2002).
- ³⁹ T. Chatterji, B. Frick, M. Zamponi, M. Appel, H. S. Nair, R. Pradheesh, G. R. Hariprya, V. Sankaranarayanan, and K. Sethupathi, Phys. Rev. B **98**, 094429 (2018).

TABLE I. The atomic coordinates and lattice parameters of $\text{La}_2\text{FeCoO}_6$ at 300 K and 1.5 K in $R\bar{3}c$ and $Pnma$ space groups respectively. The structural phase transition to $Pnma$ occurs at $T_S \approx 200$ K. The lattice parameters at 300 K (for $R\bar{3}c$) are $a = 5.4935(2)$ (Å), $c = 13.2343(2)$ (Å) and at 1.5 K (for $Pnma$) are $a = 5.4379(5)$ (Å), $b = 7.7055(6)$ (Å) and $c = 5.4886(3)$ (Å). W stands for Wyckoff position. The goodness-of-fit are χ^2 (300 K) = 2.1 and χ^2 (1.5 K) = 2.

300 K	$W.$	x	y	z
La	$6a$	0	0	0.25
Fe	$6b$	0	0	0
Co	$6b$	0	0	0
O	$18e$	0	0.4461(2)	0.25
1.5 K	$W.$	x	y	z
La	$4c$	0.0170(9)	0	0.25
Fe	$4b$	0	0	0.5
Co	$4b$	0	0	0.5
O1	$4c$	0.4935(6)	0.25	0.0631(7)
O2	$8d$	0.2697(6)	0.0385(3)	0.7304(2)
		300 K	1.5 K	
Co-O _{ap}		1.9541(12)	1.9577(2)	
Co-O _{eq}			1.961(4)	
Fe-O _{ap}		1.9541(12)	1.9577(2)	
Fe-O _{eq}			1.961(4)	
$\langle \text{Fe-O}_{ap}\text{-Co} \rangle$			159.30(3)	
$\langle \text{Fe-O}_{eq}\text{-Co} \rangle$			160.41(12)	

TABLE II. The gyromagnetic ratio, g , and the linewidth, ΔH_{pp} at different temperatures for $\text{La}_2\text{FeCoO}_6$ (LFCO) compared with the values for the disordered counterparts, $\text{Sr}_2\text{FeCoO}_6$ (SFCO) and SrLaFeCoO_6 (SLFCO).

T (K)	SFCO	LFCO	SLFCO
	$g, \Delta H_{\text{pp}}$ (G)	$g, \Delta H_{\text{pp}}$ (G)	$g, \Delta H_{\text{pp}}$ (G)
60	1.90, 4306(2)	16.07, 552(1)	2.70, 4110(4)
40	2.02, 4053(2)	20.41, –	2.65, 3741(2)
20	2.03, 4111(2)	22.02, –	2.75, 3952(2)

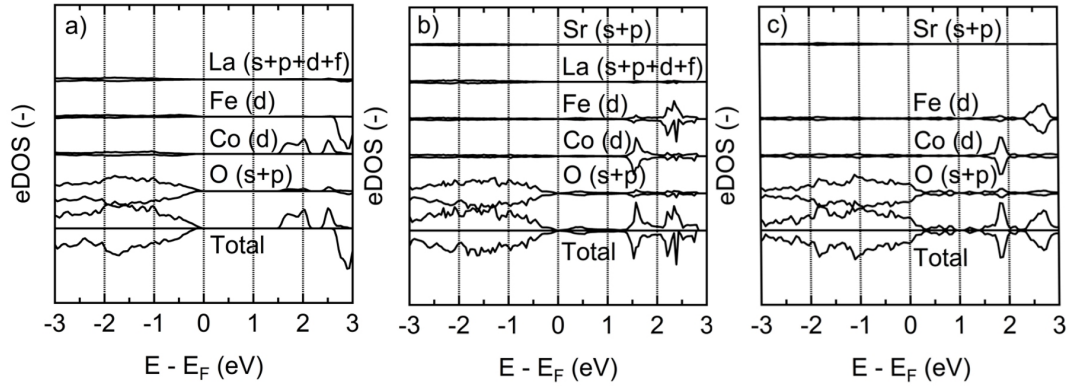


FIG. 1. The total electronic density of states (eDOS) of the ground state for (a) LFCO (G-structure), (b) SLFCO (C-structure) and (c) SFCO (G-structure) obtained through density functional theory calculations.

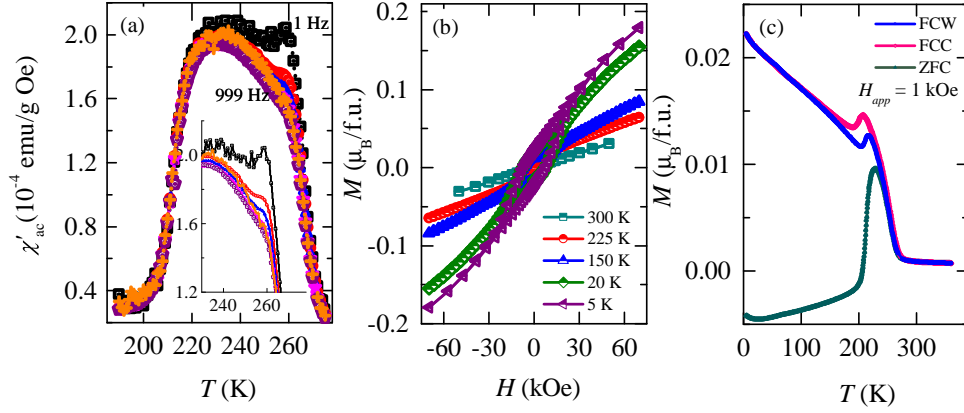


FIG. 2. (color online) (a) The real part of ac susceptibility, $\chi_{ac}(T)$, of $\text{La}_2\text{FeCoO}_6$ measured at different frequencies in the range, 1 Hz – 999 Hz. The phase transitions at T_N and T_S are evident. The inset shows a magnified view. (b) The magnetization isotherms at 5 K, 20 K, 150 K, 225 K and 300 K supports antiferromagnetism. (c) The dc magnetization FCW and ZFC shows a large bifurcation below T_S , where a thermal hysteresis is seen.

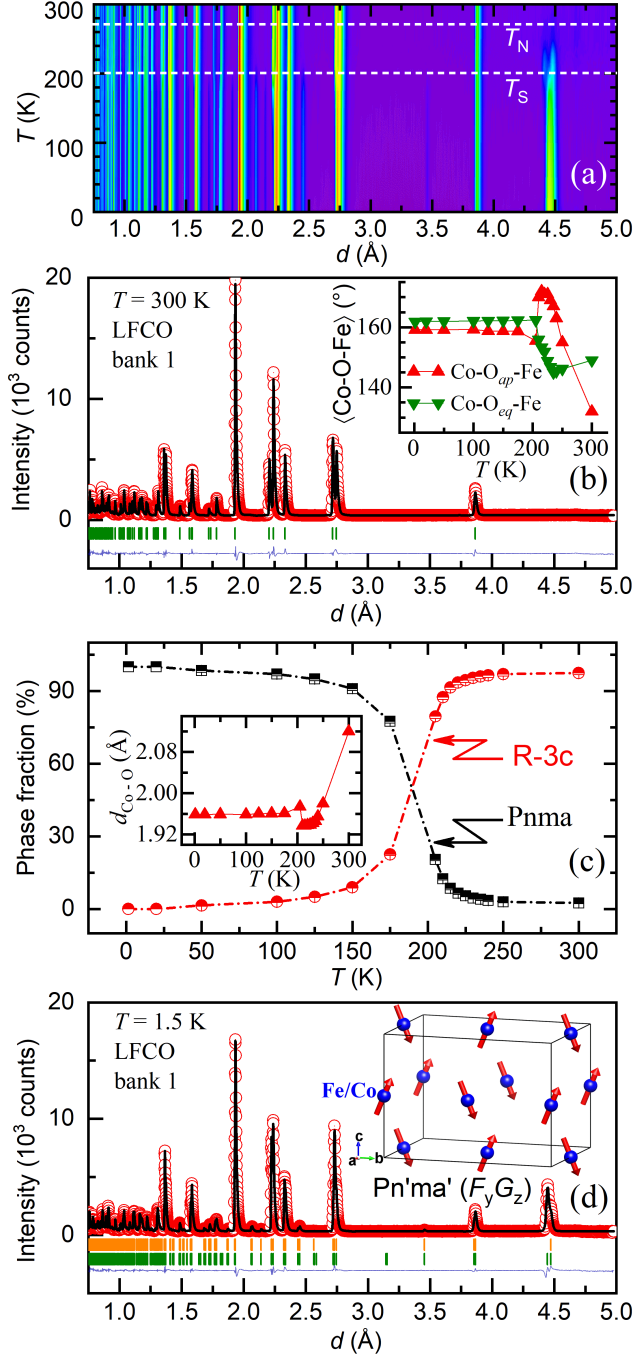


FIG. 3. (color online) (a) A 2D contour of diffracted intensity from $\text{La}_2\text{FeCoO}_6$ plotted as a function of temperature and d -spacing. A magnetic phase transition occurs in LFCO at $T_N \approx 270$ K and a structural transformation from $R\bar{3}c$ to $Pnma$ at $T_S \approx 200$ K. (b) The Rietveld refinement of the neutron powder diffraction data at 300 K. The inset shows the temperature variation of bond angles. (c) The percentage distribution of the two structural phases as a function of temperature. The bond distance as a function of temperature is shown in the inset. (d) The Rietveld refinement of the diffraction pattern at 1.5 K where the magnetic structure is faithfully accounted for by the antiferromagnetic Γ_5 representation (shown in the inset).

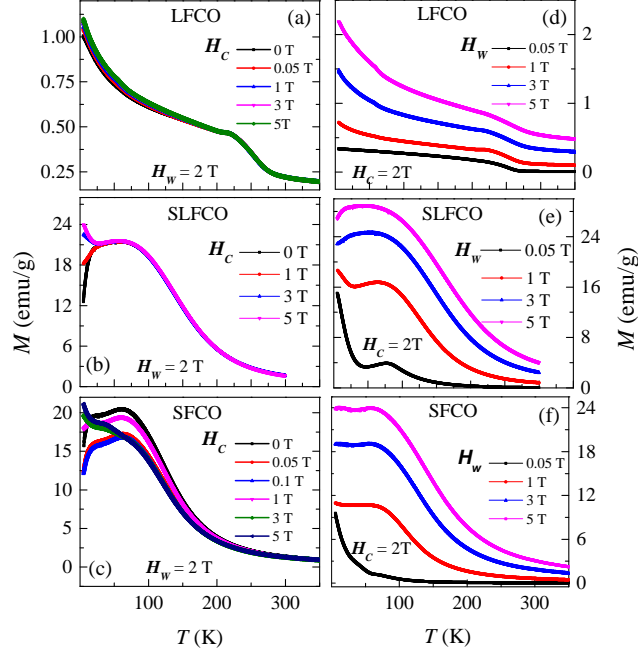


FIG. 4. (color online) Magnetization curves obtained from performing a CHUF protocol on $\text{La}_2\text{FeCoO}_6$ (a, d), SrLaFeCoO_6 (b, e) and $\text{Sr}_2\text{FeCoO}_6$ (c, f). In the panels on the left (a, b, c), a constant warming-field $H_w = 2$ T was used (CHUF1 protocol) whereas the panels on the right (d, e, f) show curves obtained with a constant cooling-field $H_c = 2$ T (CHUF2 protocol). Non-equilibrium features are visible in the magnetization of SFCO and SLFCO.

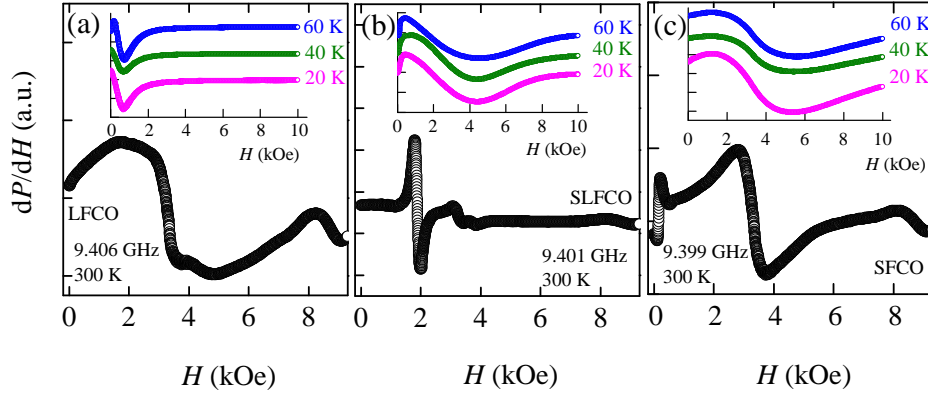


FIG. 5. (color online) The electron paramagnetic resonance curves at 300 K for (a) $\text{La}_2\text{FeCoO}_6$, (b) SrLaFeCoO_6 and (c) $\text{Sr}_2\text{FeCoO}_6$. The inset in each panel show the corresponding curves at low temperatures, 60 K, 40 K and 20 K.